Linear combination of bulk bands method for investigating the low-dimensional electron gas in nanostructured devices

David Esseni and Pierpaolo Palestri
DIEGM, Via delle Scienze 208, 33100 Udine, Italy
(Received 12 April 2005; revised manuscript received 11 July 2005; published 27 October 2005)

This paper concerns the determination of the band structure of physical systems with reduced dimensionality with the method of the linear combination of bulk band (LCBB), according to the full-band energy dispersion of the underlying crystal. The derivation of the eigenvalue equation is reconsidered in detail for quasi-two-dimensional (2D) and quasi-one-dimensional (1D) systems and we demonstrate how the choice of the volume expansion in the three-dimensional reciprocal lattice space is important in order to obtain a separated eigenvalue problem for each wave vector in the unconstrained plane (for 2D systems) or in the unconstrained direction (for 1D systems). The clarification of the expansion volume naturally leads to identification of the 2D and 1D first Brillouin zone (BZ) for any quantization direction. We then apply the LCBB approach to the silicon and germanium inversion layers and illustrate the main features of the energy dispersion and the 2D first BZ for the [001], [110], and [111] quantization directions. We further compare the LCBB energy dispersion with the one obtained with the conventional effective mass approximation (EMA) in the case of (001) silicon inversion layers. As an interesting result, we show that the LCBB method reveals a valley at the edge of the 2D first BZ which is not considered by the EMA model and that gives a significant contribution to the 2D density of states.

DOI: 10.1103/PhysRevB.72.165342 PACS number(s): 71.15.−m

I. INTRODUCTION

In modern microelectronic and optoelectronic devices, semiconductor materials are frequently structured at truly nanometric dimensions in order to exploit the properties of the low dimensional systems.[1–3] Traditional examples are quantum well based high electron mobility transistors (HEMT) based on III-V compound semiconductors; more recently, however, silicon nanostructures have been studied and fabricated even in the mainstream complementary metal-oxide-semiconductor (CMOS) technology. Prominent examples include fully depleted silicon on insulator (SOI) metal-oxide-semiconductor field-effect transistors (MOSFETs) realized on ultrathin silicon films (with thicknesses below 5 nm),[4–7] which are credible device architectures for the sub-50 nm CMOS technologies[8,9] as well as silicon nanowire transistors (SNWT), which are promising candidates for the ultimate CMOS downscaling.[10–14]

In these SOI MOS and nanowire transistors the electron gas is forced to form a quasi-two-dimensional (2D) or a quasi-one-dimensional (1D) system in the semiconductor because of the very large confining potential energy produced by the oxide (about 3 eV for the case of the SiO_2-Si system), but the electrons within the 2D or the 1D subbands can reach several hundreds of meV, so that a realistic description of the energy dispersion in the quantized system is an essential ingredient for any physically based transport model.

Traditionally, the energy dispersion in quantized systems has been calculated by using the effective mass approximation (EMA), which, for each minimum of the 3D crystal energy dispersion, expands the wave function by using only the Bloch functions corresponding to the minimum.[15,16] The main merit of the EMA is that, when a parabolic energy dispersion is assumed and only the lowest 3D band is included in the calculation, a Schrödinger-like equation can be written in the real space, which leads to simple analytical expressions for the 2D density of states and group velocities. Such expressions have been almost universally used to calculate the scattering rates and simulate the transport properties of silicon-based MOS transistors in the framework of the semiclassical approach.[17,18] The inadequacies of the EMA approach when an energy description throughout the 2D Brillouin zone (BZ) is needed have been clearly pointed out in Ref. 19.

Among the methods that can overcome the limitations of the EMA quantization model, the tight-binding (TB) approach is based on the expansion of the wave function in terms of atomic orbitals as originally proposed in Ref. 20. In its empirical formulation the TB method relies on the use of many fitting parameters to reproduce the band structure of the crystal, however, in the vast literature on the TB method several approaches have been proposed to accomplish an *ab initio* determination of the matrix elements and of the overlap integrals that enter the TB calculations (Ref. 21, and references therein).

A promising alternative to the TB procedure is the expansion of the unknown wave function as a linear combination of bulk band (LCBB), that is as a combination of the bulk Bloch functions of the constituent semiconductor.[16,19,22] Differently from the EMA approach, the expansion now includes all the states of the underlying semiconductor lattice. As neatly pointed out in Ref. 22 the expansion in terms of Bloch functions is much more physically motivated than a simple expansion in plane waves[23] and, furthermore, the ordering of the basis functions with a band index makes it easier and physically transparent to set the criterion to retain or drop the terms in the expansion. This approach has been recently used both for quantum wells and quantum dots formed with III-V compound semiconductors[19,24] and for silicon based MOS transistors.[25,26]

Although simple in its basic formulation, a correct and reliable application of the LCBB method requires one to satisfy nontrivial constraints on the states **K** of the reciprocal lattice space to be included in the expansion. More precisely, given the completeness of the Bloch functions, on the one hand it is necessary to include all the Bloch states of the underlying crystal but on the other hand one should not include bulk states that differ by a reciprocal lattice vector because this would produce an undesired overcompleteness in the expansion.

As it will be discussed in detail in Sec. II, for the 1D and the 2D systems the above constraints should be carefully considered in relation to the possibility of writing a separated eigenvalue problem for each in-plane wave vector (for the 2D systems) or for each wave vector in the unconstrained direction (for the 1D systems). The clarification of the above issues is closely related to the identification of the Brillouin zone for the 2D and the 1D systems and, in our opinion, it has not been fully documented in the previous literature.[22,24,25]

This work is essentially focused on the application of the LCBB expansion to silicon and germanium inversion layers in MOS transistors and it presents original contributions concerning the following points: (i) the derivation of the eigenvalue problem for 2D systems is rediscussed in detail and it is clarified that an appropriate choice of the expansion volume V_{EK} in the reciprocal lattice space is necessary to obtain a separated eigenvalue problem for each in-plane wave vector; (ii) the discussion concerning V_{EK} naturally leads to the definition of the 2D first BZ and to the procedure for its identification in arbitrary crystal orientation; (iii) we calculate and show the 2D first BZ for both silicon and germanium in the three main quantization directions [001], [110], and [111]; (iv) we show specific differences between the LCBB and the EMA results for silicon inversion layers in the [001] quantization direction that demonstrate the existence of a third valley (besides the *unprimed* and *primed* valleys considered by the EMA), and illustrate the contribution of such a valley to the overall 2D density of states; and (v) the discussion of an appropriate expansion volume V_{EK} mentioned at points (i) and (ii) is illustrated also for the 1D systems.

II. QUANTIZATION MODEL

Throughout the paper we write the real space vectors in terms of the 2D and the 1D component as $\mathbf{R}=(\mathbf{r},z)$ and adopt the same notation for the wave vectors $\mathbf{K}=(\mathbf{k},k_z)$ and the reciprocal lattice vectors $\mathbf{G}=(\mathbf{g},g_z)$, in fact this notation is convenient to explicitly discuss the cases of a confining potential virtually constant in a plane (2D systems) or in a direction (1D systems). Furthermore, we assume a single material approximation where H_0 is the Hamiltonian corresponding to the kinetic part and the periodic crystalline potential and $U(\mathbf{r},z)$ is the confining potential superimposed to the crystalline one. For semiconductor-oxide heterojunctions, where the band discontinuity is very large, the use of a confining potential $U(\mathbf{r},z)$ to mimic the band discontinuity seems a reasonable approximation.

Thus, under the above assumptions, the *unknown* eigenfunction ψ must satisfy the Scrödinger equation:

$$[H_0 + U(\mathbf{r},z)]\psi = \varepsilon\psi(\mathbf{r},z). \tag{1}$$

Given the completeness of the Bloch functions $\Phi_{n\mathbf{k}k_z} = |n\mathbf{k}\mathbf{k_z}\rangle$, the *unknown* eigenfunction ψ can be expanded as

$$\psi = \sum_{n',(\mathbf{k}',k_z')} A_{n'}(\mathbf{k}',k_z')\Phi_{n'\mathbf{k}'k_z'}, \tag{2}$$

where each Bloch function can be written using its corresponding periodic part $u_{n\mathbf{k}k_z}(\mathbf{r},z)$ as

$$\Phi_{n'\mathbf{k}'k_z'} = |n'\mathbf{k}'k_z'\rangle = u_{n'\mathbf{k}'k_z'}(\mathbf{r},z)e^{j\mathbf{k}'\cdot\mathbf{r}}e^{jk_z'z} \tag{3}$$

and the $u_{n'\mathbf{k}'k_z'}$, given its periodicity in the real space, can always be expressed by means of a Fourier series with components $B_{n\mathbf{k}k_z}$ as

$$u_{n'\mathbf{k}'k_z'}(\mathbf{r},z) = \frac{1}{\sqrt{V}}\sum_{(\mathbf{g},g_z)} B_{n'\mathbf{k}'k_z'}(\mathbf{g},g_z)e^{j\mathbf{g}\cdot\mathbf{r}}e^{jg_zz}, \tag{4}$$

where V is the volume of the crystal.

By projecting on the generic state $|n\mathbf{k}\mathbf{k_z}\rangle$ the Schrödinger equation becomes[16]

$$E_{FB}^{(n)}(\mathbf{k},k_z)A_n(\mathbf{k}k_z) + \sum_{n',(\mathbf{k}',k_z')} \langle n\mathbf{k}k_z|U(\mathbf{r},z)|n'\mathbf{k}'k_z'\rangle A_{n'}(\mathbf{k}',k_z') = \varepsilon A_n(\mathbf{k},k_z), \tag{5}$$

where ε is the eigenvalue and $E_{FB}^{(n)}$ is the energy corresponding to the Bloch function $\Phi_{n\mathbf{k}k_z}$. In the expansion of the unknown wave function ψ in terms of Bloch functions that has lead to Eq. (5) the wave vectors $\mathbf{K}=(\mathbf{k},k_z)$ must vary within an appropriate expansion volume V_{EK}. More precisely, given the completeness of the Bloch functions, we can choose as V_{EK} any volume such that

$$\forall(\mathbf{k},k_z),(\mathbf{k}',k_z') \in V_{EK}:$$

$$(\mathbf{k}' \neq \mathbf{k}+\mathbf{g}) \text{ or } (k_z' \neq k_z + g_z) \quad \forall\, \mathbf{G} = (\mathbf{g},\mathbf{g_z}). \tag{6}$$

The first BZ of the 3D crystal is clearly a possible choice but, as discussed in detail below, it is not necessarily the most convenient one for the 2D and the 1D systems.

Let us now consider the matrix elements of the confining potential:

$$\langle n\mathbf{k}k_z|U(\mathbf{r},z)|n'\mathbf{k}'k_z'\rangle = \int_V u^*_{n\mathbf{k}k_z}u_{n'\mathbf{k}'k_z'}U(\mathbf{r},z)e^{j(\mathbf{k}'-\mathbf{k})\cdot\mathbf{r}}e^{j(k_z'-k_z)z}d\mathbf{r}dz, \tag{7}$$

where we can use the series expansion of the $u_{n\mathbf{k}k_z}$ to obtain:

$$\langle n\mathbf{k}k_z|U(\mathbf{r},z)|n'\mathbf{k}'k_z'\rangle = \frac{1}{V}\sum_{(\mathbf{g_2},g_{2z})}\sum_{(\mathbf{g_1},g_{1z})} B^*_{n\mathbf{k}k_z}(\mathbf{g_1},g_{1z})B_{n'\mathbf{k}'k_z'}(\mathbf{g_2},g_{2z}) \times \int_V U(\mathbf{r},z)e^{j(\mathbf{k}'-\mathbf{k}+\mathbf{g_2}-\mathbf{g_1})\cdot\mathbf{r}}e^{j(k_z'-k_z+g_{2z}-g_{1z})z}d\mathbf{r}dz. \tag{8}$$

By defining $(\mathbf{g_3}, g_{3z}) = (\mathbf{g_2} - \mathbf{g_1}, g_{2z} - g_{1z})$, Eq. (8) can be rewritten as

$$\langle n\mathbf{k}k_z|U(\mathbf{r},z)|n'\mathbf{k}'k_z'\rangle = \sum_{(\mathbf{g_2},g_{2z})} \sum_{(\mathbf{g_3},g_{3z})} B^*_{n\mathbf{k}k_z}(\mathbf{g_2}-\mathbf{g_3}, g_{2z}-g_{3z}) B_{n'\mathbf{k}'k_z'}(\mathbf{g_2}, g_{2z}) \times \frac{(2\pi)^3}{V} U_T(\mathbf{k}'-\mathbf{k}+\mathbf{g_3}, k_z'-k_z+g_{3z}), \quad (9)$$

where we have introduced the Fourier transform of the confining potential:

$$U_T(\mathbf{q},q_z) = \frac{1}{(2\pi)^3}\int_V U(\mathbf{r},z) e^{j\mathbf{q}\cdot\mathbf{r}} e^{jq_z z} d\mathbf{r}dz. \quad (10)$$

Since the U_T in Eq. (9) does not depend on $(\mathbf{g_2}, g_{2z})$, we can finally write

$$\langle n\mathbf{k}k_z|U(\mathbf{r},z)|n'\mathbf{k}'k_z'\rangle = \frac{(2\pi)^3}{V} \sum_{(\mathbf{g_3},g_{3z})} S^{(n,n')}_{\mathbf{k}k_z\mathbf{k}'k_z'}(\mathbf{g_3}, g_{3z}) \times U_T(\mathbf{k}'-\mathbf{k}+\mathbf{g_3}, k_z'-k_z+g_{3z}), \quad (11)$$

where we have defined:

$$S^{(n,n')}_{\mathbf{k}k_z\mathbf{k}'k_z'}(\mathbf{g},g_z) = \sum_{(\mathbf{g}',g_z')} B^*_{n\mathbf{k}k_z}(\mathbf{g}'-\mathbf{g}, g_z'-g_z) B_{n'\mathbf{k}'k_z'}(\mathbf{g}', g_z'). \quad (12)$$

It is shown in Appendix A that $S^{(n,n')}_{\mathbf{k}k_z\mathbf{k}'k_z'}$ can be interpreted as an overlap integral between the periodic parts of appropriate Bloch functions:

$$S^{(n,n')}_{\mathbf{k}k_z\mathbf{k}'k_z'}(\mathbf{g},g_z) = \langle u_{n(\mathbf{k}-\mathbf{g})(k_z-g_z)}|u_{n'\mathbf{k}'k_z'}\rangle. \quad (13)$$

For a generic confining potential that does not have any translational invariance, as in the case of quantum dots, the expression for the matrix elements cannot be further simplified and when Eq. (11) is inserted in Eq. (5) we find an eigenvalue problem that couples all the $\mathbf{K}=(\mathbf{k},k_z)$ used for the expansion. Clearly any possible volume expansion V_{EK} satisfying Eq. (6) provides the same set of eigenvalues.

However for 2D and 1D systems the symmetries of the confining potential can be used to simplify the problem.

A. Quasi-2D systems

For a confining potential $U(\mathbf{r},z) \simeq U(z)$ which is constant in the $\mathbf{r}$ plane normal to the confining direction z, Eq. (11) simplifies to

$$\langle n\mathbf{k}k_z|U(z)|n'\mathbf{k}'k_z'\rangle = \frac{(2\pi)}{L} \sum_{(\mathbf{g},g_z)} S^{(n,n')}_{\mathbf{k}k_z\mathbf{k}'k_z'}(\mathbf{g},g_z) U_T(k_z'-k_z+g_z)\delta_{\mathbf{k},\mathbf{k}'+\mathbf{g}}, \quad (14)$$

where $U_T(q_z)$ denotes the 1D Fourier transform with respect to z and L is the length of the sample in the z direction.

We now remember that the matrix elements of Eq. (14) must be inserted in Eq. (5) where a sum must be taken over all the $(\mathbf{k}',k_z')$ in the volume V_{EK} of the reciprocal lattice space used for the wave-function expansion. When the sum over $(\mathbf{k}',k_z')$ is performed, the presence of $\delta_{\mathbf{k},\mathbf{k}'+\mathbf{g}}$ eliminates most of the terms of the sum over $(\mathbf{g},g_z)$ that are present in the expression of the matrix elements. In fact in the sum over $(\mathbf{g},g_z)$ of Eq. (14) we can isolate the term for $\mathbf{G}=(\mathbf{g},g_z)=(\mathbf{0},0)$, and then further separate, in the rest of the sum, the reciprocal lattice vectors in the quantization direction $\mathbf{G}_z=(\mathbf{0},G_z)$ (i.e., those which have a zero in-plane component $\mathbf{g}=0$) and those that have a non-null in-plane component $\mathbf{G}_{nz}=(\mathbf{g}\neq\mathbf{0},g_z)$. The capital letter G_z for the k_z component of the $\mathbf{G}_z$ vectors is used to remind us that it is the component of a vector of the reciprocal lattice along k_z (i.e., $|\mathbf{G}_z|=|G_z|$), whereas the symbol g_z has been used for the k_z component of any generic $\mathbf{G}$.

By introducing these three groups of terms in Eq. (14) and then substituting for the matrix elements in the sum over $(n',\mathbf{k}',k_z')$ of Eq. (5), we obtain:

$$\sum_{n',(\mathbf{k}',k_z')} A_{n'}(\mathbf{k}',k_z')\langle n\mathbf{k}k_z|U(z)|n'\mathbf{k}'k_z'\rangle = \frac{2\pi}{L}\sum_{n',k_z'} A_{n'}(\mathbf{k},k_z') S^{(n,n')}_{\mathbf{k}k_z\mathbf{k}k_z'}(\mathbf{0},0) U_T(k_z'-k_z) + \frac{2\pi}{L}\sum_{n',k_z'} A_{n'}(\mathbf{k},k_z') \sum_{\mathbf{G}_z=(\mathbf{0},G_z\neq 0)} S^{(n,n')}_{\mathbf{k}k_z\mathbf{k}k_z'}(\mathbf{0},G_z) U_T(k_z'-k_z+G_z) + \frac{2\pi}{L}\sum_{n',(\mathbf{k}',k_z')} A_{n'}(\mathbf{k}',k_z') \sum_{\mathbf{G}_{nz}=(\mathbf{g}\neq\mathbf{0},g_z)} \delta_{\mathbf{k},\mathbf{k}'+\mathbf{g}} S^{(n,n')}_{\mathbf{k}k_z\mathbf{k}'k_z'}(\mathbf{g},g_z) U_T(k_z'-k_z+g_z). \quad (15)$$

The first two terms in Eq. (15) depend on a single value $\mathbf{k}$ of the in-plane wave vector and contain a sum over all the values k_z' included in the expansion volume V_{EK}. The third term instead deserves a specific discussion, because, depending on the choice for V_{EK}, it can be either null or non-null. In fact it is important to remember that $\mathbf{G}_{nz}=(\mathbf{g},g_z)$ is a reciprocal lattice vector (whose in-plane component is $\mathbf{g}\neq\mathbf{0}$), however *this does not necessarily imply*

that $(\mathbf{g},0)$ *is itself a reciprocal lattice vector*.

Clearly, if $(\mathbf{g},0)$ *is a reciprocal lattice vector* (as it is the case for those $\mathbf{G}_{nz}$ that have $g_z=0$), then for any possible choice of V_{EK} satisfying Eq. (6) no $\mathbf{K}'=(\mathbf{k}',k_z')$ can exist in V_{EK} such that $\mathbf{k}=(\mathbf{k}'+\mathbf{g})$, hence the $\delta_{\mathbf{k},\mathbf{k}'+\mathbf{g}}$ zeroes all the terms in the sum over $\mathbf{k}'$. However, if $(\mathbf{g},0)$ *is not a reciprocal lattice vector*, then the third term in Eq. (15) can be non-null for some $(\mathbf{k}',k_z')\in V_{EK}$.

Simple examples when this latter case occurs can be easily identified if we take the V_{EK} equal to the first BZ of the 3D crystal, we consider face-centered-cubic (fcc) crystals (i.e., silicon, germanium, GaAs) and we assume a [001] quantization direction. In fact, if we now consider the in-plane wave vector $\mathbf{k}=(0.5,0.5)$ (throughout the paper we express the wave vectors and the vectors of the reciprocal lattice in unit of $2\pi/a_0$, where a_0 is the lattice constant), then we know that $\mathbf{K}=(\mathbf{k},k_z)$ belongs to the first BZ of the 3D crystal for $|k_z|\leqslant 0.5$. Furthermore, we can easily see that all the $\mathbf{K}'=(\mathbf{k}',k_z')$ having $\mathbf{k}'=(-0.5)$ and $|k_z'|\leqslant 0.5$ on the one hand belong to the first BZ (hence to the V_{EK}) and on the other hand satisfy $\mathbf{k}=(\mathbf{k}'+\mathbf{g})$ for $\mathbf{G}_{nz}=(\mathbf{g},g_z)=(1,1,-1)$, thus contributing to the third term in Eq. (15). More in general, for the eight reciprocal lattice vectors $\mathbf{G}_{nz}$, which have $G_{nz}=|\mathbf{G}_{nz}|=\sqrt{3}$, the corresponding vectors $(\mathbf{g},0)$ are not reciprocal lattice vectors and thus result in non-null contributions to the third term in Eq. (15). The same is true for all the reciprocal lattice vectors obtained by adding a $\mathbf{G}_z$ vector to the above eight $\mathbf{G}_{nz}$.

It should be noticed that, when Eq. (15) is substituted in Eq. (5), if no terms with $\mathbf{k}'\neq\mathbf{k}$ are present, then a separated eigenvalue problem is obtained for each in-plane wave vector $\mathbf{k}$. When the third term in Eq. (15) is non-null, instead, different in-plane wave vectors are involved in the same eigenvalue problem. We hereafter demonstrate that this can be avoided by an appropriate choice of the expansion volume V_{EK}, different from the first BZ.

In fact, for a quasi-2D electron gas, it is convenient to define V_{EK2} such that:

$$\forall(\mathbf{k},k_z),(\mathbf{k}',k_z')\in V_{EK2}:\begin{cases}\mathbf{k}'\neq\mathbf{k}+\mathbf{g} & \forall\,\mathbf{G}_{nz}=(\mathbf{g}\neq\mathbf{0},g_z)\\ k_z'\neq k_z+G_z & \forall\,\mathbf{G}_z=(\mathbf{0},G_z).\end{cases}\tag{16}$$

Clearly all the wave vectors belonging to the V_{EK2} defined by Eq. (16) satisfy even Eq. (6), so that the above definition of V_{EK2} is perfectly legitimate and theoretically equivalent to any other legitimate choice, such as the first BZ of the 3D crystal.

It is important to notice that the condition imposed by the $\mathbf{G}_{nz}$ vectors in Eq. (16) sets a constraint on the in-plane components of the wave vector belonging to the V_{EK2} such that *the third term in* Eq. (15) *is null*. Consequently, the final form for the eigenvalue problem for a 2D system becomes:

$$E_{FB}^{(n)}(\mathbf{k},k_z)A_n(\mathbf{k},k_z)+\frac{2\pi}{L}\sum_{n',k_z'}\left\{U_T(k_z'-k_z)S^{(n,n')}_{\mathbf{k}k_z\mathbf{k}k_z'}(\mathbf{0},0)+\sum_{\mathbf{G}_z=(\mathbf{0},G_z\neq 0)}U_T(k_z'-k_z+G_z)S^{(n,n')}_{\mathbf{k}k_z\mathbf{k}k_z'}(\mathbf{0},G_z)\right\}A_{n'}(\mathbf{k},k_z')=\epsilon(\mathbf{k})A_n(\mathbf{k},k_z),\tag{17}$$

where $S^{(n,n')}_{\mathbf{k}k_z\mathbf{k}k_z'}(\mathbf{0},G_z)$ is the overlap integral defined in Eq. (13). As it can be seen, Eq. (17) represents a separated eigenvalue problem for each value of the in-plane wave vector $\mathbf{k}$. This is reflected in the notation $\epsilon(\mathbf{k})$, which underlines the fact that each set of eigenvalues obtained by Eq. (17) can be associated to $\mathbf{k}$, so that by varying $\mathbf{k}$ we can describe the energy dispersion of the quasi-2D electron gas. The range where k_z must vary for the solution of Eq. (17) is set by Eq. (16).

In this regard, the condition on the $\mathbf{G}_{nz}$ vectors in Eq. (16) sets, as already said, a constraint on the in-plane components $\mathbf{k}$ of the wave vectors belonging to V_{EK2}, whereas the condition on the $\mathbf{G}_z$ sets the range of k_z. Hence Eq. (16) defines the V_{EK2} as a prism with the shape of the base set by the condition on the $\mathbf{G}_{nz}$ and the height equal to the periodicity interval in the quantization direction that is equal to the magnitude G_{zm} of the smallest reciprocal lattice vector $\mathbf{G}_z$ along the k_z direction. In particular, for the V_{EK2} centered in the origin $(\mathbf{0},0)$ of the reciprocal lattice space the k_z values simply satisfy $|k_z|\leqslant 0.5G_{zm}$. For the [001] quantization direction in fcc crystals we have $G_{zm}=2$ and the base of the V_{EK2} centered in $(\mathbf{0},0)$ is the 2D Wigner-Seitz cell formed with the in-plane components of the eight reciprocal lattice vectors $\mathbf{G}_{nz}$ that have $|\mathbf{G}_{nz}|=\sqrt{3}$. The resulting shape is the square illustrated in Fig. 1(a).

As it will be demonstrated in Appendix B the solution of the eigenvalue problem written in Eq. (17) is independent of the center of the k_z range as long as this range is equal to G_{zm} and, furthermore, the eigenvalue problem obtained for any in-plane $\mathbf{k}_{ex}$ lying *outside* the base of the V_{EK2} centered in $(\mathbf{0},0)$ is equivalent to the problem written for an appropriate $\mathbf{k}_{in}$ *inside* the base. *This demonstrates that the base of the* V_{EK2} *centered in* $(\mathbf{0},0)$ *is the first BZ for the 2D system*. For the [001] quantization direction the first BZ is thus given by the square in Fig. 1(a), whereas the shape and the area of the 2D first BZ for different quantization directions will be discussed in Sec. III B.

Before moving to the 1D systems, a further comment about Eq. (17) and its relation to the volume expansion V_{EK2} is in order. While discussing Eq. (15) we have seen that the choice of V_{EK2} given in Eq. (16) is necessary to obtain a separated eigenvalue problem for each in-plane $\mathbf{k}$. However, this choice of V_{EK2} must be equivalent to any other choice satisfying Eq. (6), such as the first BZ of the 3D crystal. At

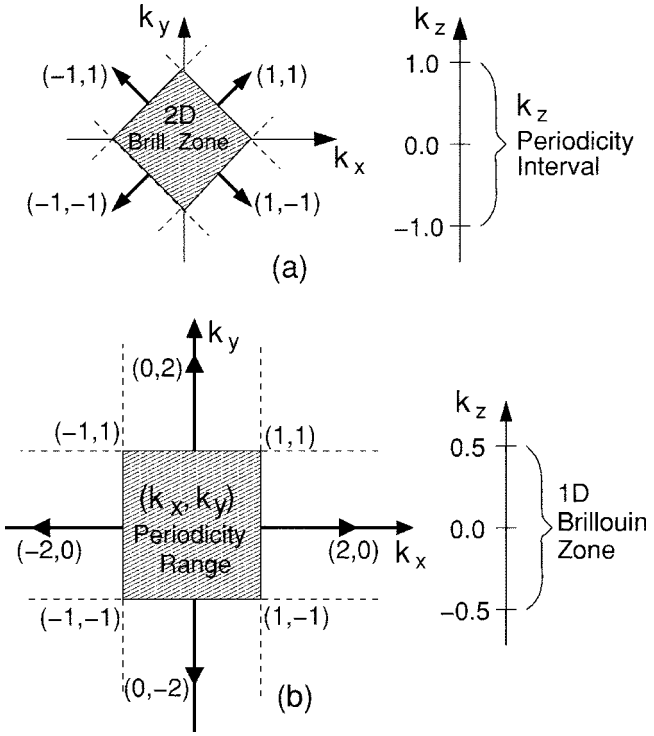

FIG. 1. (a) Quasi-2D gas: 2D first BZ (obtained as the Wigner-Seitz cell built with the in-plane components of the reciprocal lattice vectors $\mathbf{G}_{nz}$ that have $|\mathbf{G}_{nz}|=\sqrt{3}$) and the corresponding k_z range to be used in the eigenvalue problem of Eq. (17). (b) Quasi-1D gas: range of the in-plane $\mathbf{k}$ values to be used in the eigenvalue problem Eq. (21) (obtained as the Wigner-Seitz cell built with the smallest in-plane reciprocal lattice vectors $\mathbf{G}_p$) and the corresponding 1D first BZ. The quantization direction is [001].

this regard we can certainly solve the eigenvalue problem for the 2D system by using the first BZ as V_{EK2}, but, in this case, the third term in Eq. (15) does not vanish for most in-plane wave vectors, so that we have to write and solve an eigenvalue problem that includes more than one $\mathbf{k}$ value and the corresponding vectors $\mathbf{K}=(\mathbf{k},k_z)$ in the first BZ. This approach is much less attractive from a practical viewpoint than the one based on Eq. (16), although theoretically equivalent to it, because of the coupling between different $\mathbf{k}$ and even because the corresponding range of k_z values to be included in the solution becomes $\mathbf{k}$ dependent.

It is *incorrect*, instead, to write a separated eigenvalue problem for each $\mathbf{k}$ as in Eq. (17) and then limit k_z so that $\mathbf{K}=(\mathbf{k},k_z)$ belongs to the first BZ. This latter approach is inconsistent with the derivation of Eq. (17) and we verified that it leads to energy dispersions which, differently from the ones discussed in Sec. III, *are not periodic* versus the in-plane wave vector $\mathbf{k}$.

B. Quasi-1D systems

For a confining potential $U(\mathbf{r},z)\simeq U(\mathbf{r})$, which is constant in the direction z normal to a quantization plane $\mathbf{r}$, Eq. (11) simplifies to:

$$\langle n\mathbf{k}k_z|U(\mathbf{r})|n'\mathbf{k}'k_z'\rangle=\frac{(2\pi)^2}{A}\sum_{(\mathbf{g},g_z)}S^{(n,n')}_{\mathbf{k}k_z\mathbf{k}'k_z'}(\mathbf{g},g_z)U_T(\mathbf{k}'-\mathbf{k}+\mathbf{g})\delta_{k_z,k_z'+g_z}, \tag{18}$$

where $U_T(\mathbf{q})$ denotes the 2D Fourier transform in the quantization plane $\mathbf{r}$ and A is the area of the crystal in the plane $\mathbf{r}$.

Similarly to the procedure applied to Eq. (14), in the sum of Eq. (18) we can isolate the term for $\mathbf{G}=(\mathbf{g},g_z)=(\mathbf{0},0)$, and then further separate, in the rest of the sum, the reciprocal lattice vectors that belong to the quantization plane $\mathbf{G}_p=(\mathbf{g}_p\neq\mathbf{0},0)$ (i.e., those that have $g_z=0$) and those that have a non-null g_z component $\mathbf{G}_{np}=(\mathbf{g},g_z\neq 0)$. By introducing these three groups of terms in Eq. (18) and then substituting for the matrix elements in the sum over $(n',\mathbf{k}',k_z')$ of Eq. (5), we obtain:

$$\begin{aligned}\sum_{n'(\mathbf{k}',k_z')}A_{n'}(\mathbf{k}',k_z')\langle n\mathbf{k}k_z|U(\mathbf{r})|n'\mathbf{k}'k_z'\rangle=&\frac{(2\pi)^2}{A}\sum_{n',\mathbf{k}'}A_{n'}(\mathbf{k}',k_z)S^{(n,n')}_{\mathbf{k}k_z\mathbf{k}'k_z}(\mathbf{0},0)U_T(\mathbf{k}'-\mathbf{k})\\&+\frac{(2\pi)^2}{A}\sum_{n',\mathbf{k}'}A_{n'}(\mathbf{k}',k_z)\sum_{\mathbf{G}_p=(\mathbf{g_p}\neq\mathbf{0},0)}S^{(n,n')}_{\mathbf{k}k_z\mathbf{k}'k_z}(\mathbf{g_p},0)U_T(\mathbf{k}'-\mathbf{k}+\mathbf{g_p})\\&+\frac{(2\pi)^2}{A}\sum_{n',(\mathbf{k}',k_z')}A_{n'}(\mathbf{k}',k_z')\sum_{\mathbf{G}_{np}=(\mathbf{g},g_z\neq\mathbf{0})}\delta_{k_z,k_z'+g_z}S^{(n,n')}_{\mathbf{k}k_z\mathbf{k}'k_z'}(\mathbf{g},g_z)U_T(\mathbf{k}'-\mathbf{k}+\mathbf{g}).\end{aligned} \tag{19}$$

The first two terms in Eq. (19) depend on a single value of k_z and contain a sum over all the values $\mathbf{k}'$ included in the expansion volume V_{EK}. The third term is always null if the volume expansion V_{EK1} for the 1D gas is defined such that

$$\forall(\mathbf{k},k_z),(\mathbf{k}',k_z')\in V_{EK1}:\begin{cases}k_z'\neq k_z+g_z & \forall\mathbf{G}_{np}=(\mathbf{g},g_z\neq 0)\\ \mathbf{k}'\neq\mathbf{k}+\mathbf{g_p} & \forall\mathbf{G}_p=(\mathbf{g}_p,0),\end{cases} \tag{20}$$

so that the final form for the eigenvalue problem of the 1D system becomes

$$E_{FB}^{(n)}(\mathbf{k},k_z)A_n(\mathbf{k},k_z)+\frac{(2\pi)^2}{A}\sum_{n',\mathbf{k}'}\left\{U_T(\mathbf{k}'-\mathbf{k})S^{(n,n')}_{\mathbf{k}k_z\mathbf{k}'k_z}(\mathbf{0},0)+\sum_{\mathbf{G}_p=(\mathbf{g_p}\neq\mathbf{0},0)}U_T(\mathbf{k}'-\mathbf{k}+\mathbf{g_p})S^{(n,n')}_{\mathbf{k}k_z\mathbf{k}'k_z}(\mathbf{g}_p,0)\right\}A_{n'}(\mathbf{k}',k_z)=\epsilon(k_z)A_n(\mathbf{k},k_z). \tag{21}$$

As it can be seen, Eq. (21) represents a separated eigenvalue problem for each k_z and this is also implied by the notation $\epsilon(k_z)$, so that by varying k_z we can describe the energy dispersion of the quasi-1D gas. The range where $\mathbf{k}$ must vary for the solution of Eq. (21) is set by Eq. (20). At this regard, the condition on the $\mathbf{G}_{np}$ vectors in Eq. (20) sets a constraint on the k_z component of the wave vectors belonging to V_{EK1}, whereas the condition on the $\mathbf{G}_p$ sets the range of the in-plane wave vector $\mathbf{k}$. Similarly to Eq. (16), even Eq. (20) defines the V_{EK1} as a prism with the shape of the base set by the condition on the $\mathbf{G}_p$ and the height equal to the minimum component g_{zm} of a reciprocal lattice vector $\mathbf{G}_{np}$ that *does not* belong to the quantization plane (i.e., with $g_{zm}\neq 0$). In particular, for the V_{EK1} centered in the origin $(\mathbf{0},0)$ of the reciprocal lattice space the k_z values simply satisfy $|k_z|\leqslant 0.5g_{zm}$. For the [001] quantization direction we have $g_{zm}=1$ and the base of the V_{EK1} centered in $(\mathbf{0},0)$ is the 2D Wigner-Seitz cell formed with the four in-plane reciprocal lattice vectors $\mathbf{G}_p$, which have the minimum magnitude $|\mathbf{G}_p|=2$. The resulting shape is the square illustrated in Fig. 1(b).

It should be noted that the prisms corresponding to V_{EK2} and V_{EK1} are different. However in both cases the volume is 4.0 in units of $(2\pi/a_0)^3$ and it is the same as the volume of the first BZ of the 3D crystal. In fact all the expansion volumes that satisfy Eq. (6) must have the same extension.

In Appendix B it is demonstrated that the results of Eq. (21) are independent of the point where the range of the in-plane wave vectors $\mathbf{k}$ is centered (i.e., the center of the base of the prism that describes the V_{EK1}) and that, furthermore, the eigenvalue problem obtained for any k_{zex} value such that $|k_{zex}|>0.5g_{zm}$ is equivalent to the problem written for an appropriate k_{zin} with $|k_{zin}|\leqslant 0.5g_{zm}$. *This demonstrates that the range $|k_z|\leqslant 0.5g_{zm}$ is the first BZ for the 1D system*. As said above, for the [001] direction we have $g_{zm}=1$ and the range of the $\mathbf{k}$ vectors that must be included in the eigenvalue problem of Eq. (21) is illustrated in Fig. 1(b).

III. APPLICATION OF THE QUANTIZATION MODEL TO 2D SYSTEMS

The formalism developed in the previous section has been applied to the study of both silicon and germanium inversion layers in thin semiconductor films. All the simulations have been obtained assuming that the confining potential at the semiconductor-oxide interface is abrupt and with a barrier height of 3 eV. We verified that, in the cases studied in this work, the results are independent of the barrier height for barriers larger than approximately 2 eV.

A. The calculation procedure

All the results shown in the following have been obtained by solving directly Eq. (17) for the two lowest 3D conduction bands and, differently from some previous studies,[17,24] we did not introduce any simplifying assumption for the calculation of the overlap integrals and we did not drop the sum over $\mathbf{G}_z=(\mathbf{0},G_z)$. More precisely, for each in-plane $\mathbf{k}$ and for $|k_z|\leqslant 0.5G_{zm}$, we used the well-established nonlocal-pseudopotential (NLP) method to determine both the full-band dispersion $E_{FB}^{(n)}(\mathbf{k},k_z)$ and the Fourier components $B_{n\mathbf{k}k_z}$ of the $u_{n,\mathbf{k},k_z}$ functions for the underlying 3D crystal. The coefficients $B_{n\mathbf{k}k_z}$ were then used to calculate the overlap integrals $S^{(n,n')}_{\mathbf{k}k_z\mathbf{k}k'_z}(\mathbf{0},G_z)$ as indicated in Eq. (12). The parameters for the NLP procedure were taken from Ref. 27 for silicon and from Ref. 28 for germanium and a cutoff energy of 15 Ry was used for all the calculations.

Before presenting the results, two more comments are in order. The first remark is that it is very difficult and questionable to make any *a priori* assumption on the overlap integrals that enter Eq. (17) because, as illustrated in Fig. 2, their values change significantly when k_z varies over a periodicity interval. In particular the simplification $S^{(n,n')}_{\mathbf{k}k_z\mathbf{k}k'_z}\simeq\delta_{n.n'}$, which has been recently embraced or discussed by other authors, is clearly inapplicable.[17,24]

A second important point concerns the sum over $\mathbf{G}_z=(\mathbf{0},G_z)$ in Eq. (17). In this regard it has been sometimes assumed that, if the confining potential is slowly varying in a unit cell of the crystal, then $|U_T(k'_z-k_z+G_z)|$ is much smaller than $|U_T(k'_z-k_z)|$ so that the above sum can be neglected with respect to the first term in the brackets of Eq. (17).[25] However, since k_z varies in a periodicity interval $[-0.5G_{zm},0.5G_{zm}]$, the difference (k'_z-k_z) can be similar to G_{zm}, so that $|U_T(k'_z-k_z+G_z)|$ can be much larger rather than much smaller than $|U_T(k'_z-k_z)|$ for $\mathbf{G}_z=(\mathbf{0},\pm G_{zm})$. Clearly the dropping of the sum over $(\mathbf{0},G_z\neq 0)$ *is not justified* when k_z varies in a periodicity interval. In this regard it is also interesting to notice that, by recalling Eq. (14), the terms in the brackets of Eq. (17) can be immediately recognized as the matrix element $\langle n\mathbf{k}k_z|U(z)|n'\mathbf{k}'_z\rangle$. In Appendix B we show that this fact is necessary to demonstrate that the results of Eq. (17) do not depend on the center of the k_z range employed for the solution. However, the dropping of the sum in the brackets of Eq. (17) corresponds to a truncation in the calculation of $\langle n\mathbf{k}k_z|U(z)|n'\mathbf{k}'_z\rangle$ that does no longer guarantee a solution independent of the center of the k_z range.

In practice, we verified that the sum over $\mathbf{G}_z$ in the brackets of Eq. (17) converges to a stable value when at least the

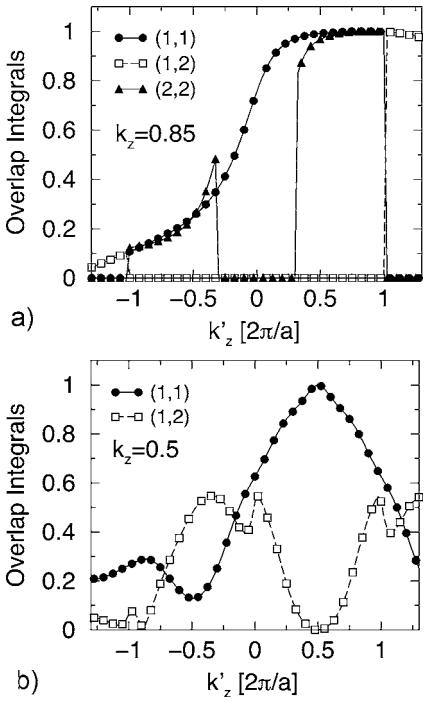

FIG. 2. Magnitude of the overlap integrals $|S^{(n,n')}_{\mathbf{k}k_z\mathbf{k}'k'_z}(\mathbf{g},g_z)|$ as defined in Eq. (12) and calculated with the NLP method and for $(\mathbf{g},g_z)=(\mathbf{0},0)$. The integrals are plotted versus k'_z for fixed values of k_z, $\mathbf{k}$, and $\mathbf{k}'$. (a) Silicon: $k_z=0.85$ and $\mathbf{k}=\mathbf{k}'=(0,0)$. (b) Germanium: $k_z=0.5$ and $\mathbf{k}=\mathbf{k}'=(0.5,0.5)$.

first two terms corresponding to $\mathbf{G}_z=(\mathbf{0},\pm G_{zm})$ are included, and that, in this case, the solution of Eq. (17) is independent of the center of the k_z range. On the contrary, when the entire sum in the brackets is dropped the results of Eq. (17) *do depend* on the center of the k_z range employed for the calculation, thus exhibiting a behavior unacceptable from both a theoretical and a practical standpoint. All the results illustrated in the remainder of the paper have been obtained by keeping the first two terms in the sum over $\mathbf{G}_z$ of Eq. (17).

As for the numerical solution of Eq. (17), the sum over the discrete k_z values (multiplied by $2\pi/L$) can be readily converted to an integral over a continuum variable k_z, which is in turn calculated as a discretized sum. The results illustrated in the following have been typically obtained with a k_z spacing of $\Delta k_z=0.025$ and we verified that the results are unaffected by a further reduction of the discretization step.

B. Silicon and germanium inversion layers for different crystal orientations

In this section we illustrate the calculated in-plane energy dispersion for silicon and germanium corresponding to a 5 nm thick semiconductor film and for different quantization directions. For such a thickness, the lowest subbands for the silicon inversion layers stem from the Δ valleys of the 3D conduction band, while they stem from the Λ valleys for the germanium inversion layers. The results illustrated in this section pertain to an ideal well in the sense that the potential in the semiconductor film is constant.

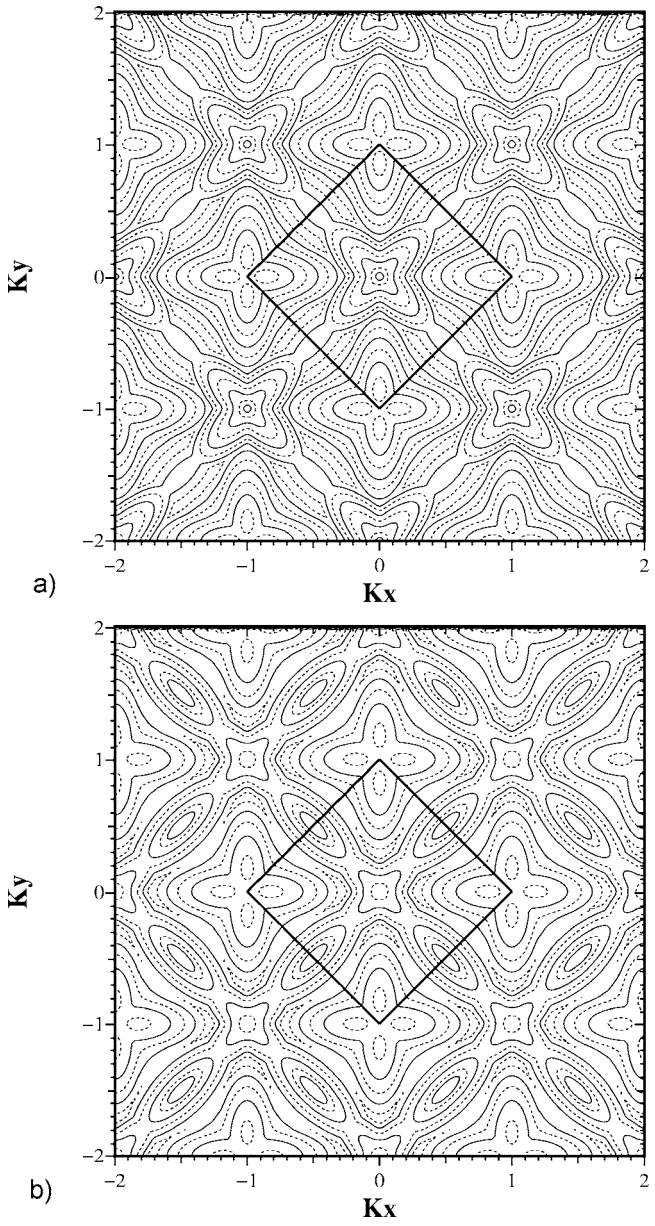

FIG. 3. (a) Silicon, [001] quantization direction. Contour plots of the energy versus in-plane $\mathbf{k}$ for the lowest eigenvalue. The energy values are 0.04, 0.3, 0.85, 1.45, 2.05, and 2.65 [eV] for the solid lines and 0.12, 0.55, 1.15, 1.75, and 2.35 [eV] for the dashed lines. The absolute minimum is in $\mathbf{k}=0$ and it is approximately two-time degenerate, while four more degenerate minima are in $\mathbf{k}=(0,\pm 0.85)$ and $\mathbf{k}=(\pm 0.85,0)$. (b) Same as in (a) but for germanium. The minima are in $\mathbf{k}=(\pm 0.5,\pm 0.5)$ and around these points the eigenvalues are approximately two-time degenerate. The energy values are 0.18, 0.55, 1.15, 1.75, and 2.35 [eV] for the solid lines and 0.3, 0.85, 1.45, 2.05, and 2.65 [eV] for the dashed lines. k_x and k_y are the [100] and [010] directions in the CCS. The semiconductor film thickness is 5 nm and the energy reference is the bottom of the confining potential well.

Figure 3 shows the lowest eigenvalue versus the in-plane wave vector for both silicon and germanium obtained for the [001] quantization direction. The squares in Fig. 3 indicate the calculated 2D first BZ which is fully consistent with the

TABLE I. Two independent in-plane vectors $\mathbf{g}_{B1}$ and $\mathbf{g}_{B2}$ expressed in the device coordinate system and obtained by taking the in-plane components of the reciprocal lattice vectors $\mathbf{G}_{nz}$ that have $|\mathbf{G}_{nz}|=\sqrt{3}$. The Wigner-Seitz cell built with $\mathbf{g}_{B1}$ and $\mathbf{g}_{B2}$ is the 2D first BZ for each quantization direction and this explains the results of Figs. 3–5. The table also reports the radius of the circle circumscribed to the 2D first BZ as well as the k_z range that must be used in the solution of Eq. (17) for the different quantization directions.

	$\mathbf{g}_{B1}$	$\mathbf{g}_{B2}$	Radius	k_z range
[**001**]	(1,1)	$(1,-1)$	1.0	2.0
[**110**]	(1,0)	$(0,\sqrt{2})$	$\sqrt{3}/2$	$2\sqrt{2}$
[**111**]	$(4/\sqrt{6},0)$	$(2/\sqrt{6},2/\sqrt{2})$	$2\sqrt{2}/3$	$\sqrt{3}$

shape inferred from the base of the V_{EK2} defined by Eq. (16). More precisely such a square is the Wigner-Seitz cell formed by the in-plane vectors obtained by taking the in-plane components of the $\mathbf{G}_{nz}$ that have $|\mathbf{G}_{nz}|=\sqrt{3}$. Only two of these in-plane vectors are independent and they unequivocally identify the 2D first BZ. Table I shows that two such independent vectors can be taken as $\mathbf{g}_{B1}=(1,1)$ and $\mathbf{g}_{B2}=(1,-1)$ for the [001] direction.

As for the different quantization directions, it should be noticed that the Schrödinger equation written with the LCBB method has been implicitly derived in the device coordinate system (DCS), whereas the NLP solver typically works in the crystal coordinate system (CCS).[27] In the [001] direction the CCS coincides with the DCS so that the reciprocal lattice vectors $\mathbf{G_{nz}}$ (that identify the 2D first BZ) and the $\mathbf{G_z}$ (that set the periodicity interval) are readily known. For the [110] or [111] quantization directions, instead, the vectors in the DCS must be expressed in the CCS by means of an appropriate rotation matrix. For the [110] direction the matrix is

$$\mathbf{R}_{[\mathbf{110}]}=\begin{pmatrix} 0 & 1.0/\sqrt{2} & 1.0/\sqrt{2} \\ 0 & -1.0/\sqrt{2} & 1.0/\sqrt{2} \\ 1 & 0 & 0 \end{pmatrix} \tag{22}$$

and for the [111] direction it is

$$\mathbf{R}_{[\mathbf{111}]}=\begin{pmatrix} -2/\sqrt{6} & 0 & 1.0/\sqrt{3} \\ 1/\sqrt{6} & -1/\sqrt{2} & 1.0/\sqrt{3} \\ 1/\sqrt{6} & 1/\sqrt{2} & 1.0/\sqrt{3} \end{pmatrix}. \tag{23}$$

Thus, once the rotation matrices are known, Eq. (17) can be readily solved for the different quantization directions. The range of k_z values that must be included in the solution for each in-plane $\mathbf{k}$ is given by the periodicity interval of the considered quantization direction or, equivalently, by the magnitude of the smallest $\mathbf{G}_z$: such a range is $2\sqrt{2}$ and $\sqrt{3}$ for the [110] and the [111] directions, respectively, whereas, as said above, it is 2.0 for the [001] direction.

Figures 4 and 5 show the lowest eigenvalue versus $\mathbf{k}$ for both silicon and germanium for the [110] and the [111] quantization direction, respectively: the rectangle and the hexagon indicate the calculated 2D first BZ. Even for the [110] and the [111] directions the 2D first BZ must be the Wigner-Seitz cell built with the in-plane components in the DCS of the $\mathbf{G}_{nz}$ that have $|\mathbf{G}_{nz}|=\sqrt{3}$. The easiest way to express such $\mathbf{G}_{nz}$ in the DCS is to take the vectors $\mathbf{G}=(\pm1,\pm1,\pm1)$ in the

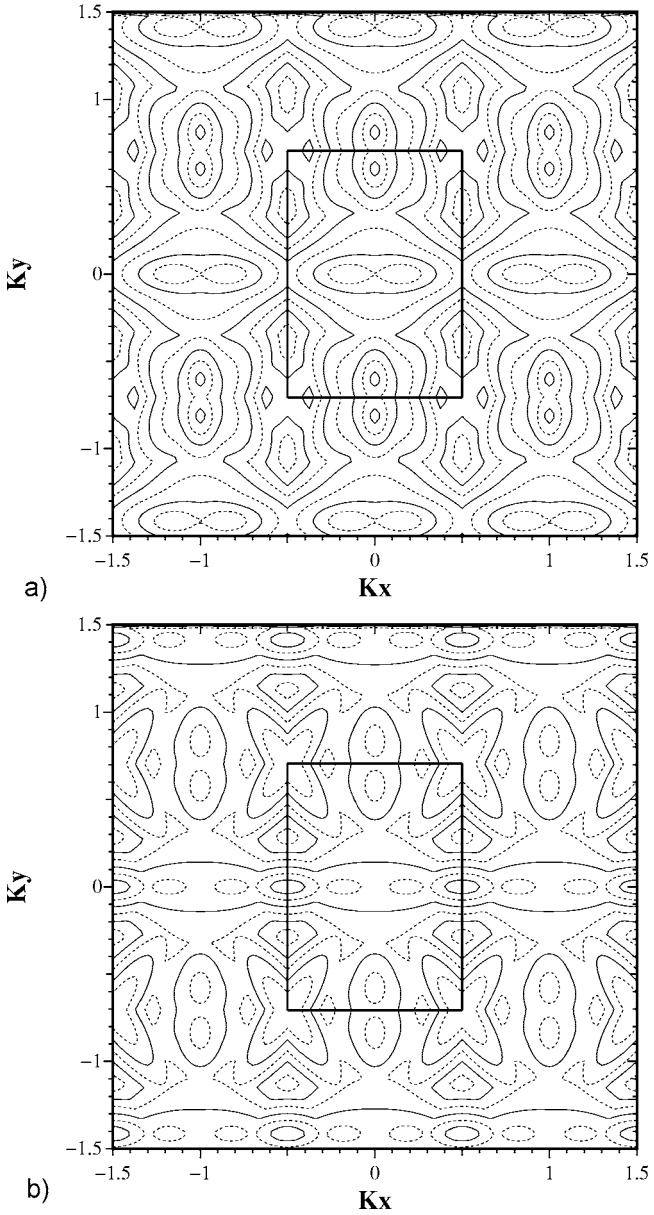

FIG. 4. (a) Silicon, [110] quantization direction. Contour plots of the energy vs in-plane $\mathbf{k}$ for the lowest eigenvalue. The absolute minima are in $\mathbf{k}=(0,\pm0.85/\sqrt{2})$ and they are approximately two-time degenerate while two more degenerate minima are in $\mathbf{k}=(\pm0.15,0)$. The energy values are 0.06, 0.3, 0.85, 1.45, 2.05, and 2.65 [eV] for the solid lines and 0.15, 0.55, 1.15, 1.75, and 2.35 [eV] for the dashed lines. (b) Same as in (a) but for germanium. The absolute minima are in $\mathbf{k}=(\pm0.5,0)$ and are approximately two-time degenerate, while four more degenerate minima are in $\mathbf{k}=(\pm0.5,\pm1/\sqrt{2})$. The energy values are 0.13, 0.55, 1.15, 1.75, and 2.35 [eV] for the solid lines and 0.3, 0.85, 1.45, 2.05, and 2.65 [eV] for the dashed lines. k_x and k_y are the [001] and $[1,\bar{1},0]$ directions in the CCS. The semiconductor film thickness is 5 nm and the energy reference is the bottom of the confining potential well.

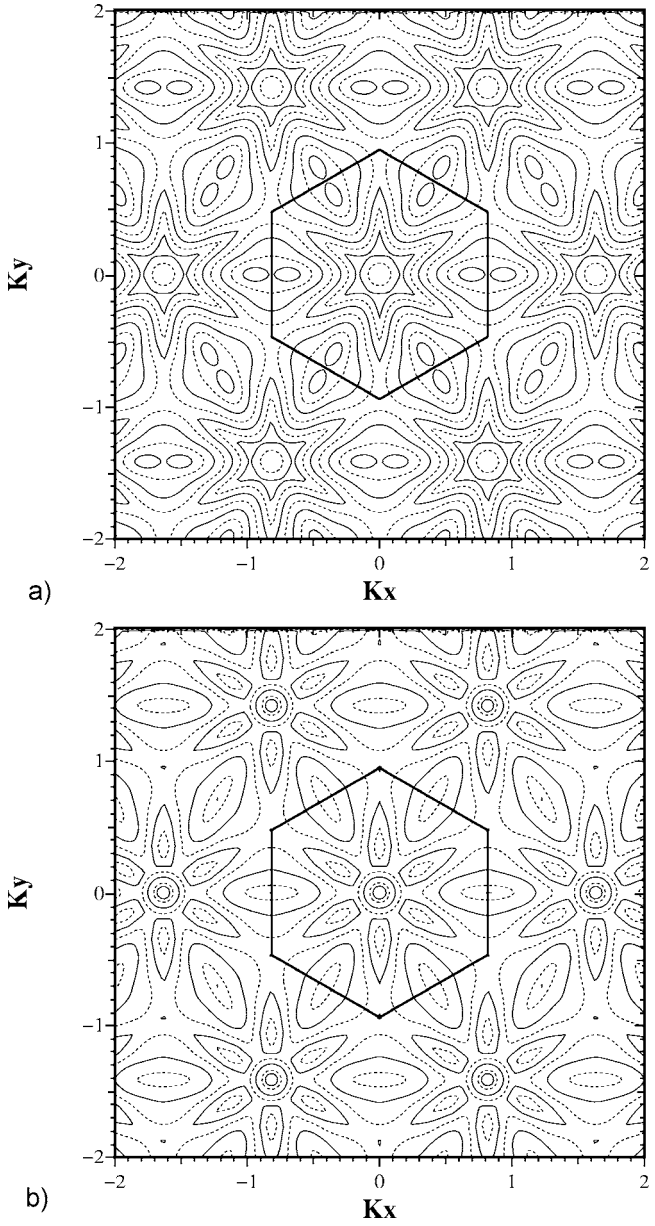

FIG. 5. (a) Silicon, [111] quantization direction. Contour plots of the energy vs in-plane **k** for the lowest eigenvalue. The minima are in $\mathbf{k}=(\pm 1.7/\sqrt{6},0)$ and in $\mathbf{k}=(\pm 0.85/\sqrt{6},\pm 0.85/\sqrt{2})$. The energy values are 0.12, 0.55, 1.15, 1.75, and 2.35 [eV] for the solid lines and 0.3, 0.85, 1.45, 2.05, and 2.65 [eV] for the dashed lines. (b) Same as in (a) but for germanium. The absolute minimum is in $\mathbf{k}=(0,0)$ and it is one-time degenerate while six more degenerate minima are in $\mathbf{k}=(\pm 2/\sqrt{6},0)$ and $\mathbf{k}=(\pm 1/\sqrt{6},\pm 1/\sqrt{2})$. The energy values are 0.12, 0.5, 1.15, 1.75, and 2.35 [eV] for the solid lines and 0.25, 0.85, 1.45, 2.05, and 2.65 [eV] for the dashed lines. k_x and k_y are the $[\bar{2},1,1]$ and $[0,\bar{1},1]$ directions in the CCS. The semiconductor film thickness is 5 nm and the energy reference is the bottom of the confining potential well.

CCS and transform them to the DCS. The transformation is obtained by using the inverse (i.e., the transpost) of the unitary matrices given in Eqs. (22) and (23) for the [110] and the [111] directions, respectively.

By doing so, one can calculate two independent in-plane vectors $\mathbf{g}_{B1}$ and $\mathbf{g}_{B2}$ in the DCS which univocally identify the 2D first BZ. These $\mathbf{g}_{B1}$ and $\mathbf{g}_{B2}$ vectors are reported in Table I for the different quantization directions. For the [110] and [111] directions the corresponding Wigner-Seitz cells are the rectangle and hexagon reported in Figs. 4 and 5 and thus explain the shapes of the calculated 2D first BZ. In Table I we have also reported the radius of the circle circumscribed to the 2D first BZ as well as the k_z range that must be used in the solution of Eq. (17) for the different quantization directions.

It should be noticed that, consistently with the notation of Sec. II, the **k** values in Figs. 3–5 are expressed in the DCS, and the directions of k_x and k_y in the CCS are defined by the rotation matrices used to solve Eq. (17). More precisely, for the [001] quantization direction the k_x and k_y in the CCS are simply given by the [100] and [010] directions, respectively, whereas they are given by the [001] and $[1,\bar{1},0]$ directions for the [110] quantization and finally by the $[\bar{2},1,1]$ and $[0,\bar{1},1]$ directions for the [111] quantization case.

The simulation results of Figs. 3–5 are in agreement with the 2D first BZ, the location and the degeneracy of the minima that had been qualitatively sketched in Ref. 29.

IV. FULL BAND VERSUS EFFECTIVE MASS RESULTS FOR SILICON INVERSION LAYERS

As an application of prominent applicative interest for the microelectronic industry, this section compares, for a (001) silicon inversion layer, the results calculated with the LCBB method described in the previous sections with those obtained with the simpler EMA approach. The device structure simulated is an SOI device with a silicon thickness $T_{\mathrm{Si}}=9.4$ nm and a very small acceptor type doping concentration in the silicon film $N_A=10^{15}$ cm^{-3}. The confining potential $U(z)$ used for the LCBB calculations is the self-consistent potential obtained from the Schrödinger-Poisson solver based on the EMA method. Hence the EMA and LCBB results have been obtained by using exactly the same confining potential, even because, in the present version of our LCBB solver, a self-consistent solution of the Poisson and Schrödinger problems with the LCBB method is computationally too heavy.

However, the results illustrated in the remainder of this section show that the 2D density of states (DOS) obtained with the two quantization models are essentially the same in the range of energies that are appreciably occupied at the equilibrium; consequently very modest differences are expected in the self-consistent potential obtained with either the EMA or the LCBB method in the problem studied in this work.

A. Energy dispersion and valley splitting

Figure 6 illustrates the energy dispersion within the lowest *unprimed* subband $\epsilon_0(\mathbf{k})$ (i.e., around the $\mathbf{k}=\mathbf{0}$ point) in the [010] and [110] direction, where the EMA results have been calculated according to both the parabolic and the non-

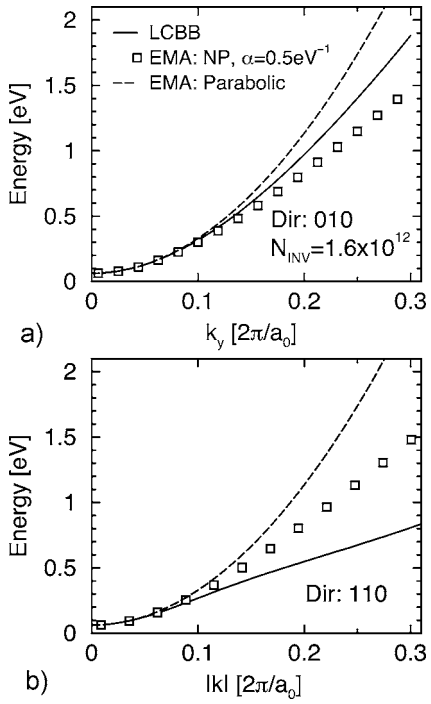

FIG. 6. (a) Energy dispersion with the LCBB and with the EMA method for $\mathbf{k}$ close to the center of the 2D first BZ, hence corresponding to the first *unprimed* subband. The EMA case results are presented for either the parabolic or the nonparabolic approximations. (a) In-plane plotting direction [010], hence $k_x=0$ and $k=|\mathbf{k}|=k_y$; and (b) in-plane plotting direction [110], hence $k_x=k_y$ and $k=|\mathbf{k}|=\sqrt{2}k_x$. Silicon with quantization direction [001]. SOI structure with $T_{\mathrm{Si}}=9.4$ nm and inversion density $N_{inv}=1.6\times10^{12}$ cm^{-2}. The energy reference is the confining potential at the front Si-oxide interface.

parabolic (NP) relation widely used in silicon transport studies:[18,30]

$$\epsilon_0(\mathbf{k})=\epsilon_{00}+\frac{1}{2\alpha}\left[-1+\sqrt{1+2\alpha\hbar^2\left(\frac{k_x^2}{m_x}+\frac{k_y^2}{m_y}\right)}\right]. \quad (24)$$

As it can be seen, the bottom of the subband $\epsilon_{00}=\epsilon_0(\mathbf{k}=\mathbf{0})$ predicted by the EMA is in very close agreement with the LCBB results and, for the [010] direction, the EMA can track quite well the LCBB energy dispersion even for $\mathbf{k}\neq\mathbf{0}$. In the [110] direction, instead, the EMA largely overestimates the energy at a given $k=|\mathbf{k}|$ and this stems from a strong anisotropy of the 3D energy dispersion E_{FB}, which is poorly reproduced by the EMA. For the *primed* minimum [i.e., around the $\mathbf{k}=(0,\pm0.85)$ point], we found that the results are similar to Fig. 6 in the [100] direction whereas a large discrepancy between the EMA and the LCBB results is found in the [010] direction (not shown).

These results can be summarized by saying that, in the range of silicon thicknesses down to about 5 nm considered in this paper, the EMA is fairly accurate as far as the bottom of the lowest subbands is concerned. However, the EMA model assumes that the dependence of the 3D energy dispersion on both k_z and $\mathbf{k}$ can be reproduced with three constant masses calculated at the minimum of the 3D dispersion.

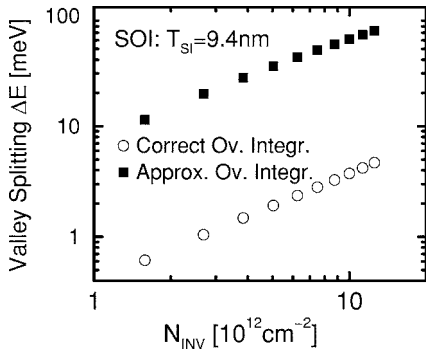

FIG. 7. Valley splitting vs N_{INV} for silicon with the [001] quantization direction. SOI structure with $T_{\mathrm{Si}}=9.4$ nm. The plotted quantity is the difference between the two lowest eigenvalues calculated for $\mathbf{k}=\mathbf{0}$ (*unprimed subband* in the EMA picture).

Consequently, significant differences between the EMA and the LCBB results emerge whenever the 3D energy curvature with respect to k_z (i.e., $\partial^2E_{FB}/\partial k_z^2$) changes with $\mathbf{k}$ or the dependence of the 3D energy on $\mathbf{k}$ deviates from the parabolic behavior at the E_{FB} minimum.

An interesting effect that cannot be captured by the EMA method is the possible splitting of the supposedly two-time degenerate *unprimed* subbands (Ref. 31, and references therein). The LCBB method naturally describes the valley splitting as an effect of the breakage of the crystal symmetry in the quantization direction produced by the confining potential. Consequently we used our LCBB solver to investigate the quantitative relevance of this splitting.

Figure 7 shows the difference between the two lowest eigenvalues calculated for $\mathbf{k}=\mathbf{0}$ and plotted versus the inversion density N_{inv}: the results indicated with the open symbols have been obtained by using the values of the overlap integrals $S^{(n,n')}_{\mathbf{k}k_z\mathbf{k}k_z'}$ provided by the NLP calculations, whereas the closed symbols have been obtained with the approximation $S^{(n,n')}_{\mathbf{k}k_z\mathbf{k}k_z'}\simeq\delta_{n,n'}$. As it can be seen, the valley splitting increases with N_{inv} and reaches about 4 meV at the largest N_{inv} of practical interest (open symbols). Since this splitting is much smaller than the thermal energy KT around room temperature, it can be quite safely neglected in the analysis of the electron devices. For the purpose of this work, however, it is interesting to see that the unjustified approximation for the overlap integrals (see Fig. 2) results in a vast exaggeration of the valley splitting. This example confirms that, as said above, it is very difficult to make *a priori* simplifications in Eq. (17) and, most of all, it is difficult to predict the consequences of these simplifications on the results.

B. Third valley in silicon inversion layers

An interesting difference between the results of the EMA and the LCBB methods concerns the energy dispersion near the edge of the 2D first BZ. In this regard Fig. 8 reports the lowest eigenvalues versus k_x calculated with the LCBB method for the [001] quantization direction and for $\mathbf{k}$ values close to the *primed* minimum located at $\mathbf{k}=(0.85,0)$. The features of the energy dispersion can be explained by con-

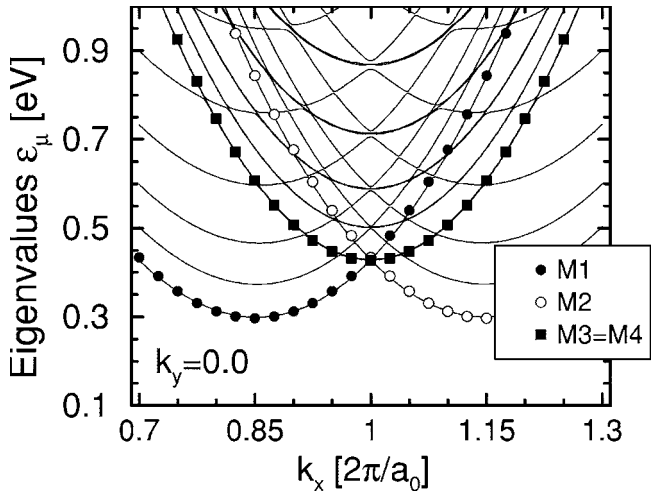

FIG. 8. Plot of some of the lowest eigenvalues $\epsilon_\mu(\mathbf{k})$ vs k_x and for $k_y=0.0$. The symbols are used *only* for the lowest branch of each set of minima. Besides the known set of *primed* minima [M1 centered in $\mathbf{k}=(0.85,0)$ and M2, which is the periodic replica of the set in $\mathbf{k}=(-0.85,0)$], an additional set of minima denoted X valley is found in $\mathbf{k}=(1.0,0)$ (M3 and M4). Each subband of this X valley is two time degenerate. The M1$\cdots$ M4 subbands cross one another at $k_x=1.0$ and the corresponding eigenvalues are four time degenerate. SOI structure with $T_{\mathrm{Si}}=9.4$ nm and inversion density $N_{inv}=1.1\times10^{13}$ cm^{-2}. The energy reference is the confining potential at the front Si-oxide interface.

sidering four families of minima denoted M1$\cdots$M4: for the sake of clarity the symbols have been used only for the lowest branch of each family. The eigenvalues for $k_x>1.0$ are just the periodical repetition of those obtained inside the 2D first BZ indicated in Fig. 3(a), in particular the minima M2 for $k_x=1.15$ correspond to the identical ones in $k_x=-0.85$. Clearly the M1 minimum for $\mathbf{k}=(0.85,0)$ is the *primed* minimum also predicted by the EMA. Furthermore, two virtually identical minima M3 and M4 located at $\mathbf{k}=(1.0,0)$ form a third valley for the 2D silicon system (besides the conventional *unprimed* and *primed* ones), hereafter denoted X-valley from the X symmetry point $(\mathbf{k},k_z)=(1.0,0,0)$ in the 3D first BZ. Such X-valleys are located at points $\mathbf{k}=(\pm1.0,0)$ and $\mathbf{k}=(0,\pm1.0)$, and each subband is essentially two time degenerate.

In order to understand the 2D energy dispersion near $\mathbf{k}=(1.0,0)$ and the origin of the X-valley in Fig. 8 it is important to remember that, according to Eq. (17), the calculation of the eigenvalues for a given $\mathbf{k}$ involves all the states of the 3D dispersion for k_z in a periodicity interval (i.e., $4\pi/a_0$ for the [001] quantization). More precisely, the numerical solution of Eq. (17) shows that each minimum of the 3D energy $E_{FB}^{(n)}$ versus k_z dispersion (which is not necessarily a minimum even along k_x and k_y), leads to a set of eigenvalues similar to those predicted by the EMA. In this regard Fig. 9(a) reports the 3D energy dispersion versus k_z and for $\mathbf{k}=(1.0,0)$ (solid lines): since the two lowest 3D conduction bands ($E_{FB}^{(1)}$ and $E_{FB}^{(2)}$) are degenerate, four identical minima versus k_z exist in the periodicity interval (M1, M2 at $k_z=0.0$ and M3, M4 at $k_z=1.0$), which explain the four time degenerate eigenvalues M1$\cdots$M4 correspondingly obtained

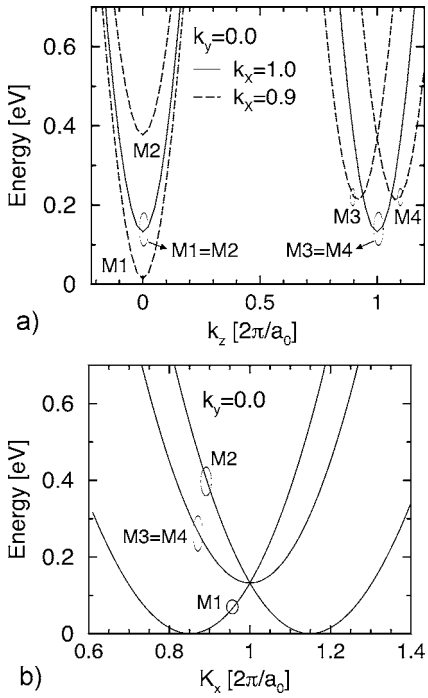

FIG. 9. (a) Energy vs k_z for the two lowest 3D bands $E_{FB}^{(1)}$ and $E_{FB}^{(2)}$ and for either $\mathbf{k}=(1.0,0)$ (solid lines) or $\mathbf{k}=(0.9,0)$ (dashed lines). For $\mathbf{k}=(1.0,0)$ the two bands are degenerate and the four identical minima M1$\cdots$ M4 produce the four time degenerate eigenvalues at $\mathbf{k}=(1.0,0)$ in Fig. 8. For $\mathbf{k}=(0.9,0)$, instead, $E_{FB}^{(1)}$ and $E_{FB}^{(2)}$ split, the M3 and M4 minima remain degenerate but M1 and M2 take different values. (b) The M1$\cdots$ M4 minima plotted vs k_x and for $k_y=0.0$, hence along the same direction used in Fig. 8 for the plotting of the eigenvalues $\varepsilon(\mathbf{k})$. The behavior of the eigenvalues in Fig. 8 reflects the trend of the M1$\cdots$ M4 minima.

in Fig. 8 for $\mathbf{k}=(1.0,0)$. Furthermore, Fig. 9(a) also illustrates the 3D dispersion versus k_z and for $\mathbf{k}=(0.9,0)$ (dashed lines): for this $\mathbf{k}$ value the M1 and M2 minima split whereas the M3 and M4 minima near $k_z=1.0$ remain degenerate. The above behavior of the M1$\cdots$M4 minima is best clarified in Fig. 9(b) where the minima are plotted versus k_x, hence along the same direction used in Fig. 8 for the plotting of the eigenvalues $\varepsilon(\mathbf{k})$. Clearly the M1 and M2 minima of Fig. 9(b) result in the corresponding M1 and M2 eigenvalues in Fig. 8 (closed and open circles), while the M3 and M4 minima of Fig. 9(b) produce the two time degenerate M3 and M4 eigenvalues in Fig. 8 (closed squares).

As already said, the M1 and M2 eigenvalues of Fig. 8 are provided even by the EMA model applied to the minimum of the 3D energy dispersion located in $(\mathbf{k},k_z)=(0.85,0,0)$. The X-valley centered at $\mathbf{k}=(1.0,0)$ instead stems from the full-band quantization model and it cannot be obtained by the EMA written around the minima of the 3D energy dispersion. In fact the X-symmetry point of the 3D first BZ located in $(\mathbf{k},k_z)=(1.0,0,0)$ *is not even a minimum of the 3D energy dispersion* because the gradient with respect to the $\mathbf{k}$ is non-null (i.e., $\bar{\nabla}_{\mathbf{k}}E_{FB}\neq0$). Furthermore, in the calculation of the 2D system eigenvalues the EMA considers only the states of the 3D dispersion close to a minimum, whereas the analysis of Figs. 8 and 9 has shown that the X valley does not stem

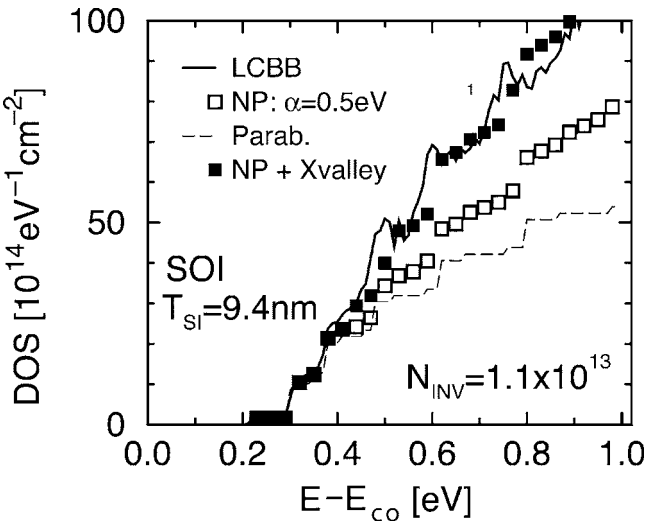

FIG. 10. Two-dimensional density of states vs energy. The full-band quantization model (solid line) leads to a DOS larger than the EMA nonparabolic model (nonparabolicity factor $\alpha=0.5$ eV^{-1}) that employs only the *unprimed* and *primed* valleys (open squares). The strictly parabolic model ($\alpha=0$) results in even lower DOS values (dashed line). A good agreement with the FB results is obtained by adding the X valley to the EMA model (closed squares). SOI structure with $T_{\mathrm{Si}}=9.4$ nm and inversion density $N_{inv}=1.1\times10^{13}$ cm^{-2}. E_{C0} is the minimum of the confining potential at the Si-oxide interface.

from states close to the X symmetry point of the first BZ but rather from the states close to the point $(\mathbf{k},k_z)=(1.0,0,1.0)$, which is the X symmetry point of the two adjacent 3D BZs centered in (1,1,1) and $(1,-1,1)$. Hence the identification of the X valley is a result inherently related to the full band quantization model.

In order to further compare the full-band and the EMA quantization models we have studied the 2D density of states (DOS). For the LCBB model the DOS has been numerically calculated by counting, for each energy bin, the **k** points in the 2D first BZ that have an eigenvalue belonging to the energy bin. Each **k** point must then be weighted for an appropriate volume in the **k** plane according to the **k** discretization. For the EMA model the analytical expressions for the DOS for both the parabolic or NP case have been reported by many authors.[1,17,18] Figure 10 compares the LCBB results (solid line) with several approximations obtained with the EMA model. As it can be seen, the conventional two-valley picture derived by the EMA approach significantly underestimates the DOS even when a nonparabolicity factor $\alpha=0.5$ eV^{-1} is used (open squares). More precisely, the LCBB DOS starts increasing above the two-valley EMA DOS exactly at the energies corresponding to the lowest minimum in the X valley.

In an attempt to improve the EMA model and reconcile it with the LCBB results, we have explicitly added to it the X valley. To this purpose, the eigenvalues in this third valley are *empirically* taken as the eigenvalues of the *primed* valley shifted upward by 130 meV. In fact we verified over a broad range of N_{INV} values and for different device structures that the minima in the X-valley are about 130 meV higher than those in the *primed* valley, a difference equal to the energy value at the X-symmetry point in the 3D energy dispersion. Furthermore, for the X valley we used a density-of-state mass $m_d=0.62$ (in fact the energy dispersion of the X valley is well fitted with $m_x=m_y=0.62m_0$—not shown), and the degeneracy was set to two, because each of the four X valleys located at points $\mathbf{k}=(0,\pm1.0)$ and $\mathbf{k}=(\pm1.0,0)$ is two time degenerate. However, Fig. 3(a) shows that approximately one-fourth of the states in each X valley belong to the 2D first BZ. It is interesting to see how the nonparabolic model with *three valleys* results in a DOS that is in very good agreement with the FB results. This fact on the one hand confirms that the discrepancy between the FB and the two valley, EMA DOS stems from the states of the X-valley, and on the other hand provides a simple, semiempirical approach to include this valley in the conventional EMA picture.

The results of this section concerning the X valley and its impact on the DOS have been confirmed for a large variety of confining potentials ranging from the simple ideal wells also used for Figs. 3–5 to both SOI and bulk MOS structures.

V. CONCLUSIONS

In this paper we have reconsidered the LCBB quantization model and discussed in detail its derivation for 2D and 1D systems. In particular we have shown that in 2D systems, if the first BZ of the 3D reciprocal lattice space is used as the expansion volume, one cannot write a separated eigenvalue problem for each in-plane wave vector **k**. To this purpose, in fact, it is necessary to choose the expansion volume V_{EK2} as the prism defined by Eq. (16).

Such a definition of the V_{EK2} naturally identifies the BZ of the 2D system and clarifies the range of k_z values in the quantization direction that one must include in the LCBB expansion at a given in-plane **k**. The expansion volume V_{EK2} and the corresponding 2D first BZ and k_z range depend on the quantization direction through the representation of the reciprocal lattice vectors in the DCS that are obtained with the appropriate rotation matrices given in Eqs. (22) and (23). Thus the above discussion about V_{EK2} results in practical guidelines for the calculation procedure, which are useful and necessary to obtain the periodicity of the energy versus **k** illustrated in Figs. 3–5. A similar discussion has been outlined also for the 1D systems.

From the application viewpoint, the calculation procedure derived from the LCBB method has been used for the 2D systems obtained with either silicon or germanium. In particular we have documented some differences between the results obtained with either the LCBB or the conventional EMA quantization model for silicon inversion layers in the [001] quantization direction. The LCBB has revealed the existence of a third valley in this 2D system located at the edge of the 2D first BZ and stemming from the X symmetry points of the 3D band structure. Our results indicate that this valley can significantly contribute to the 2D DOS for energies just a few hundreds of meV above the absolute minimum of the 2D energy dispersion relation.

ACKNOWLEDGMENTS

We would like to thank M. Pavesi, P. L. Rigolli, and F. Venturi for providing us with some of the routines used for

the NLP calculations and L. Selmi for his constant support and for helpful discussions. This work was partly supported by the Italian MIUR (FIRB project RBNE012N3X and PRIN 2004) and the EU (SINANO NoE, IST-506844).

APPENDIX A

In this appendix we shall show that the quantity $S^{(n,n')}_{\mathbf{K}K'}(\mathbf{G})$ defined in Eq. (12) can be interpreted as the overlap integral of the periodic parts of appropriate Bloch functions, where $\mathbf{K}$ and $\mathbf{G}$ denote a wave vector and a reciprocal lattice vector, respectively, of the 3D crystal. In fact, for any $\mathbf{K}$ and for any reciprocal lattice vector $\mathbf{G}$ in the reciprocal lattice, we have $u_{n\mathbf{K}+\mathbf{G}}=e^{-j\mathbf{G}\cdot\mathbf{R}}u_{n\mathbf{K}}$ that leads to:

$$u_{n\mathbf{K}+\mathbf{G}}(\mathbf{R}) = e^{-j\mathbf{G}\cdot\mathbf{R}}\frac{1}{\sqrt{V}}\sum_{\mathbf{G_1}} B_{n\mathbf{K}}(\mathbf{G_1})e^{j\mathbf{G_1}\cdot\mathbf{R}} = \frac{1}{\sqrt{V}}\sum_{\mathbf{G_1}} B_{n\mathbf{K}}(\mathbf{G_1})e^{j(\mathbf{G_1}-\mathbf{G})\cdot\mathbf{R}}, \tag{A1}$$

where $\mathbf{G_2}=(\mathbf{G_1}-\mathbf{G})$ is clearly another reciprocal lattice vector that allows us to rewrite Eq. (A1) as

$$u_{n\mathbf{K}+\mathbf{G}}(\mathbf{R}) = \frac{1}{\sqrt{V}}\sum_{\mathbf{G_2}} B_{n\mathbf{K}}(\mathbf{G_2}+\mathbf{G})e^{j\mathbf{G_2}\cdot\mathbf{R}}. \tag{A2}$$

Thus the overlap integral between $u_{n\mathbf{K}+\mathbf{G}}$ and a generic $u_{n'\mathbf{K}'}$ is given by

$$\langle u_{n\mathbf{K}+\mathbf{G}}|u_{n'\mathbf{K}'}\rangle = \sum_{\mathbf{G_1},\mathbf{G_2}} B^*_{n\mathbf{K}}(\mathbf{G_2}+\mathbf{G})B_{n'\mathbf{K}'}(\mathbf{G_1})\frac{1}{V}\int_V e^{j(\mathbf{G_1}-\mathbf{G_2})\cdot\mathbf{R}} = \sum_{\mathbf{G_1}} B^*_{n\mathbf{K}}(\mathbf{G_1}+\mathbf{G})B_{n'\mathbf{K}'}(\mathbf{G_1}) \tag{A3}$$

that finally demonstrates Eq. (13).

APPENDIX B

In this appendix we shall show that the base of the V_{EK2} centered in $(\mathbf{0},0)$ is the first BZ for the 2D systems and that the k_z extension of the V_{EK1} centered in $(\mathbf{0},0)$ is the first BZ for the 1D systems.

As for the 2D systems, by recalling Eq. (14) we can rewrite Eq. (17) as

$$E^{(n)}_{FB}(\mathbf{k},k_z)A_n(\mathbf{k},k_z) + \sum_{n',k'_z}\langle n\mathbf{k}k_z|U(z)|n'\mathbf{k}k'_z\rangle A_{n'}(\mathbf{k},k'_z) = \varepsilon(\mathbf{k})A_n(\mathbf{k},k_z), \tag{B1}$$

where $(\mathbf{k},k_z)$ belongs to the V_{EK2} centered in $(\mathbf{0},0)$, hence $|k_z|\leqslant 0.5G_{zm}$. Since both the 3D energy dispersion $E^{(n)}_{FB}(\mathbf{k},k_z)$ and the Bloch functions are periodic in k_z with a period G_{zm}, the form given in Eq. (B1) is particularly convenient to show that, if the k_z range employed in the solution of Eqs. (17) and (B1) is not centered in $k_z=0$, this implies a mere reordering of the Bloch functions used in the expansion that clearly does not change the eigenvalues. In other words, for a given in-plane vector $\mathbf{k}$, Eq. (17) must be solved by letting k_z vary in a periodicity interval and the results are independent of the center of this interval.

Let us now consider an in-plane wave vector $\mathbf{k}_{ex}$ lying outside the base of the V_{EK2} centered in $(\mathbf{0},0)$ [i.e., such that $(\mathbf{k}_{ex},0)$ does not belong to the V_{EK2} centered in $(\mathbf{0},0)$]. In this case, by the definition of V_{EK2} in Eq. (16), a reciprocal lattice vector $\mathbf{G}_{1nz}=(\mathbf{g1}\neq 0,g_{1z})$ must exist such that $\mathbf{k}_{in}=\mathbf{k}_{ex}+\mathbf{g1}$ lies inside the base of the V_{EK2} centered in $(\mathbf{0},0)$. The eigenvalue problem Eq. (B1) written for $\mathbf{k}_{ex}$ and with $|k_z|\leqslant 0.5G_{zm}$ is equivalent to the problem obtained by summing the reciprocal lattice vector $\mathbf{G}_{1nz}$ to all the wave vectors because both the energy $E^{(n)}_{FB}(\mathbf{k},k_z)$ and the Bloch functions are periodic in the reciprocal lattice of the 3D crystal. This latter eigenvalue problem resulting from the translation by $\mathbf{G}_{1nz}$ is the problem for an in-plane wave vector $\mathbf{k}_{in}=\mathbf{k}_{ex}+\mathbf{g1}$ and with $k_z\in[-0.5G_{zm}+g_{1z},0.5G_{zm}+g_{1z}]$, which is in turn equivalent to any other eigenvalue problem written for $\mathbf{k}_{in}$ and, in particular, to the one obtained by expanding in the V_{EK2} centered in $(\mathbf{0},0)$ which implies $|k_z|\leqslant 0.5G_{zm}$.

The above reasoning demonstrates that the eigenvalue problem obtained for any in-plane $\mathbf{k}_{ex}$ lying *outside* the base of the V_{EK2} centered in $(\mathbf{0},0)$ is equivalent to the problem written for an appropriate $\mathbf{k}_{in}$ *inside* the base, consequently *the base of the V_{EK2} centered in $(\mathbf{0},0)$ is the first BZ for the 2D gas*.

An entirely analogous path can be followed even for 1D systems. In fact by recalling Eq. (14) we can rewrite Eq. (21) as

$$E^{(n)}_{FB}(\mathbf{k},k_z)A_n(\mathbf{k},k_z) + \sum_{n',\mathbf{k}'}\langle n\mathbf{k}k_z|U(\mathbf{r})|n'\mathbf{k}'k_z\rangle A_{n'}(\mathbf{k}',k_z) = \varepsilon(\mathbf{k})A_n(\mathbf{k},k_z), \tag{B2}$$

where $(\mathbf{k},k_z)$ belongs to the V_{EK1} centered in $(\mathbf{0},0)$ hence $|k_z|\leqslant 0.5g_{zm}$. If the $\mathbf{k}$ range employed in the solution of Eqs. (21) and (B2) is not centered in $\mathbf{k}=0$, this results in a mere reordering of the Bloch functions $\Phi_{n\mathbf{k}k_z}$ used in the expansion, because both the 3D energy dispersion $E^{(n)}_{FB}(\mathbf{k},k_z)$ and the $\Phi_{n\mathbf{k}k_z}$ are periodic in the in-plane region identified by the smallest $\mathbf{G}_p$; i.e., the base of the V_{EK1} centered in $(\mathbf{0},0)$. Consequently the results of Eqs. (21) and (B2) are independent of the center of the $\mathbf{k}$ range.

If we now take a k_{zex} such that $|k_{zex}|>0.5g_{zm}$ a $\mathbf{G}_{1np}=(\mathbf{g1},g_{1z}\neq 0)$ must exist such that $k_{zin}=k_{zex}+g_{1z}$ has a magnitude $|k_{zin}|\leqslant 0.5g_{zm}$. The eigenvalue problem written for k_{zex} can thus be recast in the problem for k_{zin} by summing the reciprocal lattice vector $\mathbf{G}_{1np}$ to all the wave vectors involved in the solution and by exploiting the fact that the solution in k_{zin} is independent of the center of the $\mathbf{k}$ range.

This demonstrates that the eigenvalue problem for any k_{zex} with a magnitude $|k_{zex}|>0.5g_{zm}$ is equivalent to the problem written for an appropriate k_{zin} with magnitude $|k_{zin}|\leqslant 0.5g_{zm}$, consequently *the k_z range $[-0.5g_{zm},0.5g_{zm}]$ corresponding to the V_{EK1} centered in $(\mathbf{0},0)$ is the first BZ for the 1D gas*.

[1] D. K. Ferry and S. M. Goodnick, *Transport in Nanostructures* (Cambridge University Press, Cambridge, UK, 1997).
[2] S. Datta, *Electronic Transport in Mesoscopic Systems* (Cambridge University Press, Cambridge, UK, 1998).
[3] V. V. Mitin, V. A. Kochelap, and M. A. Stroscio, *Quantum Heterostructures* (Cambridge University Press, Cambridge, UK, 1999).
[4] D. Esseni, M. Mastrapasqua, G. K. Celler, C. Fiegna, L. Selmi, and E. Sangiorgi, IEEE Trans. Electron Devices **48**, 2842 (2001).
[5] D. Esseni, M. Mastrapasqua, G. K. Celler, C. Fiegna, L. Selmi, and E. Sangiorgi, IEEE Trans. Electron Devices **50**, 802 (2003).
[6] K. Uchida, J. Koga, R. Ohba, and T. S. Takagi, Tech. Dig. - Int. Electron Devices Meet. **2001**, 633 (2001).
[7] K. Uchida, H. Watanabe, A. Kinoshita, J. Koga, T. Numata, and S. Takagi, Tech. Dig. - Int. Electron Devices Meet. **2002**, 47 (2002).
[8] Y. Taur, D. A. Buchanan, W. Chen, D. J. Frank, K. E. Ismail, S.-H. Lo, G. A. Sai-Halasz, R. G. Viswanathan, H. C. Wann, S. J. Wind, and H.-S. Wong, IEEE Proc. **85**, 486 (1997).
[9] C-T. Chuang, P-F. Lu, and C. J. Anderson, IEEE Proc. **86**, 689 (1998).
[10] K. Morimoto, T. Hirai, K. Yuki, and K. Morita, Jpn. J. Appl. Phys., Part 2 **35**, 853 (1996).
[11] Y. S. Tang, G. Jin, J. H. Davies, J. G. Williamson, and C. D. W. Wilkinson, Phys. Rev. B **45**, 13799 (1992).
[12] M. Je, S. Han, I. Kim, and H. Shin, Solid-State Electron. **44**, 2207 (2000).
[13] J. Wang, E. Polizzi, and M. Lundstrom, Tech. Dig. - Int. Electron Devices Meet. **2003**, 695 (2003).
[14] C. M. Lieber, Tech. Dig. - Int. Electron Devices Meet. **2003**, 300 (2003).
[15] J. C. Slater, Phys. Rev. **76**, 1592 (1949).
[16] J. M. Luttinger and W. Kohn, Phys. Rev. **97**, 869 (1955).
[17] M. V. Fischetti and S. E. Laux, Phys. Rev. B **48**, 2244 (1993).
[18] Chr. Jungemann, A. Edmunds, and W. L. Engl, Solid-State Electron. **36**, 1529 (1993).
[19] L. W. Wang and A. Zunger, Phys. Rev. B **59**, 15806 (1999).
[20] J. C. Slater and G. F. Koster, Phys. Rev. **94**, 1498 (1954).
[21] A. Di Carlo, Semicond. Sci. Technol. **18**, R1 (2003).
[22] L. W. Wang, A. Franceschetti, and A. Zunger, Phys. Rev. Lett. **78**, 2819 (1997).
[23] L. W. Wang and A. Zunger, Phys. Rev. B **54**, 11417 (1996).
[24] F. Chirico, A. Di Carlo, and P. Lugli, Phys. Rev. B **64**, 045314 (2001).
[25] H. Takeda, N. Mori, and C. Hamaguchi, J. Comput. Electron. **1**, 467 (2002).
[26] F. Sacconi, M. Povolotskyi, A. Di Carlo, P. Lugli, and M. Stadele, Solid-State Electron. **48**, 575 (2004).
[27] J. R. Chelikowsky and M. L. Cohen, Phys. Rev. B **14**, 556 (1976).
[28] M. V. Fischetti and J. M. Higman, in *Monte Carlo Device Simulation: Full Band and Beyond*, edited by K. Hess (Kluwer, Dordrecht, 1991), Chap. 5.
[29] F. Stern and W. E. Howard, Phys. Rev. **163**, 816 (1967).
[30] C. Jacoboni and L. Reggiani, Rev. Mod. Phys. **55**, 645 (1983).
[31] T. Ando, A. Fowler, and F. Stern, Rev. Mod. Phys. **54**, 437 (1982).